AQUA
Water Infrastructure, Ecosystems and Society

IWA PUBLISHING

 AQUA — Water Infrastructure, Ecosystems and Society Vol 72 No 5, 827 doi: 10.2166/aqua.2023.051

Magnetic nanocomposites prepared from red mud and durian husk as an effective bio-adsorbent for methylene blue adsorption

Nghia T. Bui[a], Thanh Thi Hoang[b], Phuong L. N. Nguyen[b], Nguyen Thi My Linh[c], Quoc-An Trieu[d] and Trung Huu Bui[e,*]

[a] Faculty of Food Science and Technology, Ho Chi Minh City University of Food Industry, Ho Chi Minh City, Vietnam
[b] Faculty of Chemical Engineering, Industrial University of Ho Chi Minh City, Ho Chi Minh City, Vietnam
[c] Faculty of Garment Technology – Fashion, Industrial University of Ho Chi Minh City, Ho Chi Minh City, Vietnam
[d] Faculty of Environmental and Food Engineering, Nguyen Tat Thanh University, Ho Chi Minh City, Vietnam
[e] Faculty of Chemical and Food Engineering, Ho Chi Minh City University of Technology and Education, Ho Chi Minh, Vietnam
*Corresponding author. E-mail: bhtrung@hcmute.edu.vn

ABSTRACT

An increasing interest in nanocomposites prepared from agricultural/industrial byproducts has been paid for environmental remediation, especially in water treatment. This study reports the facile preparation of a low-cost magnetic biocomposite of magnetic Fe_3O_4 nanoparticles (NPs) incorporated with biopolymers extracted from durian husk, called bp-Fe_3O_4 and examined in the removal of methylene blue (MB) dye. Here, Fe_2O_3 NPs were first recovered from red mud waste and then converted to magnetic nanostructured Fe_3O_4 using a one-pot process via carbon combustion. The bp-Fe_3O_4 inherited the characteristics of each constituent component, while showing slightly higher saturation magnetization than the bare Fe_3O_4 NPs (19.84 and 18.66 emu/g, respectively), allowing for easy separation from the aqueous solution using a suitable magnet. The MB adsorption on bp-Fe_3O_4 reached an equilibrium state within 60 min reaction and achieved >90% of removal (at 50 mg/L MB) at an optimal pH range of 6–8. The effective adsorption of MB dye was attributed to both the hydroxylated-Fe_3O_4 NPs and biopolymers. The material showed excellent reusability tested up to the seventh MB adsorption cycle (decreased by <2% of adsorption efficiency). Overall, the outstanding magnetic properties and low-cost bp-Fe_3O_4 rendered them easily manipulated and separated, and reusable for water/wastewater treatment of MB dye.

Key words: adsorption, biocomposite, durian husk, magnetic nanoparticles, methylene blue

HIGHLIGHTS

- Magnetic biopolymer@Fe_3O_4 was successfully prepared from red mud and durian husk.
- Magnetic Fe_3O_4 nanoparticles were prepared using a one-pot carbon combustion.
- Good magnetic properties render them easily separated using a suitable magnet.
- Fast and effective removal of methylene blue (MB) on the biopolymer@Fe_3O_4 at pH 7.
- Good reusability of the biopolymer@Fe_3O_4 during 7 runs of MB adsorption–desorption.

GRAPHICAL ABSTRACT

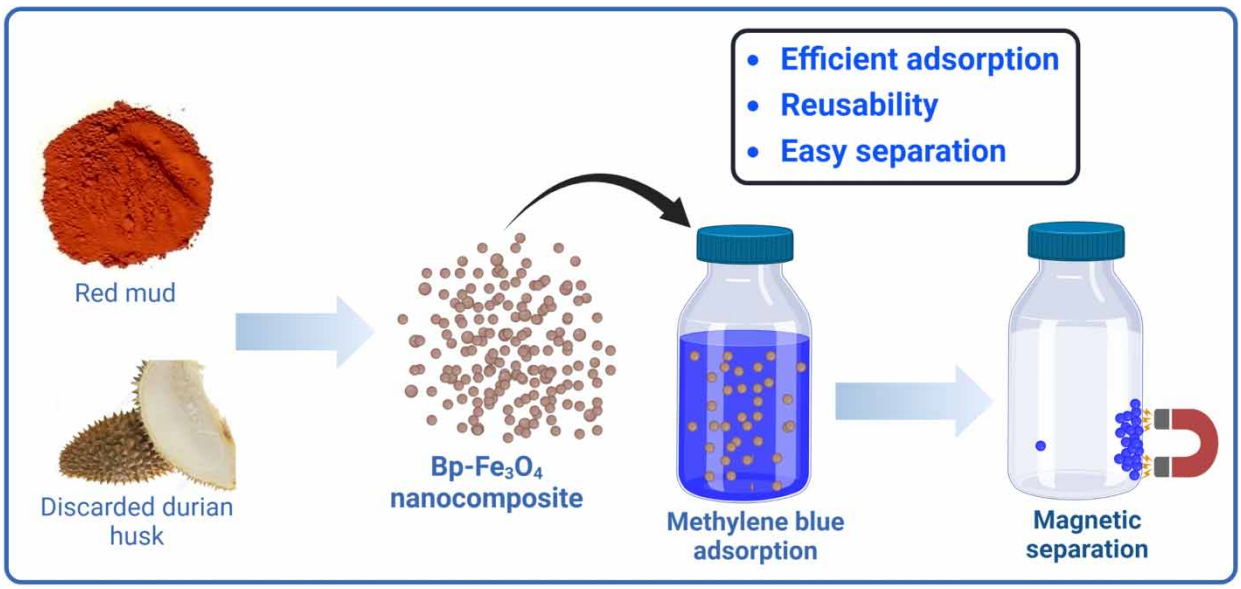

1. INTRODUCTION

Organic chemicals, especially organic dyes, are over-controlled and discharged from a variety of industrial effluents such as plastics, textiles, food, and paper which have considerably contributed to environmental pollution in recent years (Aksu *et al.* 2010; Zhou *et al.* 2014). Many toxic dye components such as aromatic compounds can resist biodegradation (Shahi *et al.* 2017) and threaten aquatic living and humans (Aksu 2005; El-Bindary *et al.* 2015). Among them, methylene blue (MB) is a common cationic dye that has received many applications including cosmetics, textiles, papers, and hygienic and health care sections. Gradual exposure to MB over a long duration of time would be harmful to human health and cause certain side effects such as difficulty in breathing, hypertension nausea, and cancer (Aksu *et al.* 2010). Therefore, it is essential to remove MB dye from contaminated water/wastewater before being discharged into the environment. So far, adsorption technology has gained great attention for MB remediation because the process is inexpensive, easy to design and operate, and has almost no formation of secondary pollutants (Rafatullah *et al.* 2010; Shitu & Ibrahim 2014; Wang *et al.* 2016; Ayalew & Aragaw 2020; Hurairah *et al.* 2020; Radoor *et al.* 2022).

The choice of adsorbent is key to determining the removal efficiency of the process. In consideration of the available diversity of adsorbents, nanomaterials have shown fascinating properties such as extremely high specific area and abundant reactive sites, which can satisfy the demand for fast kinetic adsorption and high adsorption efficiency (Alver *et al.* 2020; Bui *et al.* 2021; Ghereghlou *et al.* 2022). However, nanoparticles (NPs) tend to aggregate and reduce the surface area and active sites for the adsorption which is resulted from van der Waals forces or other interactions (Kamiya *et al.* 2018). Surface functionalization/incorporation with suitable chemicals or surfactants could allow for nanomaterials to stabilize in a dispersing medium, with sufficient repulsive force against the van der Waals forces. Although nanomaterials exhibit exclusive properties over conventional materials, efforts have been made to separate them during/after the adsorption process. Recently, magnetic metal oxide NPs having outstanding magnetic response and electronic structure have been extensively studied for various applications (Bardajee & Hooshyar 2014; Mohebbi *et al.* 2018) due to their advantages of a short-time reaction, easy manipulation, and feasibility to separate from solution by applying a magnetic field.

Based on the above discussions, the study aims to develop a magnetic biocomposite of Fe_3O_4 NPs recovered from red mud incorporated with biopolymer extracted from a durian husk, called bp-Fe_3O_4, as a low-cost bio-adsorbent for the removal of MB dye from water. The material is expected to exhibit a high adsorption capacity toward MB owing to NP size and the ease of separation from the aqueous medium by using an external magnetic field (Kuai *et al.* 2013). Red mud is known as a huge source of solid waste discarded from the production of alumina from bauxite ores via the Bayer process (Brunori *et al.* 2005), estimated up to 1.5 tons of red mud per each ton of alumina product. Annually, approximately 70 Mt of red mud is generated

globally due to the increasing demand for alumina in industrial activities (Vangelatos *et al.* 2009; Liu & Zhang 2011), and about 5.0 Mt is estimated in Vietnam particularly (Hai *et al.* 2014). It causes a huge challenge to utilize this massive volume of red mud waste and reduce the environmental impacts of its disposal (Nguyen *et al.* 2022). Red mud contains a rich source of inorganic minerals including, remaining aluminum, iron, silica, and calcium (Rivas Mercury *et al.* 2011). Of those, iron accounts for the largest percentage reaching up to 50% in oxide forms (Paramguru *et al.* 2004; Zhang *et al.* 2011). Thus, efforts have extensively focused on red mud as an iron-bearing resource for iron recovery (Piga *et al.* 1993). Regarding agricultural byproducts, durian husk is a waste produced from processing durian fruit (*Durio zibethinus*), a highly valued and desired tropical fruit indigenous to Southeast Asia and Vietnam particularly (Hokputsa *et al.* 2004). It is noted that the husk usually represents more than half of the total fruit mass and contains a high amount of cellulose, hemicellulose, lignin, and pectin (Hokputsa *et al.* 2004; Payus *et al.* 2021). Thus, durian husk has recently been utilized as a valuable source for environmental applications such as preparing a low-cost adsorbent for removing water hardness and total dissolved solids (Payus *et al.* 2021), lead (Ngabura *et al.* 2019), and MB dye (Sudrajat *et al.* 2021). The utilization of those agricultural and industrial byproducts for environmental reclamation could reduce their negative impact on the environment and increase value-added opportunities for agricultural/industrial products.

In this study, Fe_2O_3 NPs recovered from red mud were converted to magnetic nanostructured Fe_3O_4 using a facile and one-pot method via carbon combustion. This synthesis process can overcome the drawbacks of high-temperature conditions or long processing times as previously reported (Daou *et al.* 2006; Ni *et al.* 2009; Wu *et al.* 2011). The Fe_3O_4 NPs were then incorporated with biopolymers extracted from durian husk to form the bp-Fe_3O_4 composite. A series of instrumental analyses were used to characterize the morphologic, structural, and magnetic properties of the prepared materials. The resultant biocomposite was used to investigate the applicable adsorption of MB dye from water. The research outcome would provide a low-cost magnetic-based composite for the removal of MB dye in an eco-friendly way and productively.

2. EXPERIMENTS

2.1. Chemicals and materials

Ethylenediaminetetraacetic acid (EDTA) and MB (>82%) were purchased from Merck (Merck Millipore, Darmstadt, Germany). Granular activated carbon (CAS 64365-11-3) was purchased from Zhongju (Henan, China). Other chemicals e.g., ammonium hydroxide (NH_4OH, 25–28%), ethanol (C_2H_5OH, 99.7%), hydrochloric acid (HCl, >36%), and sodium hydroxide (NaOH, 96%) were bought from Xilong Chemicals (Guangdong, China).

Durian RI-6 fruits were bought from a local market in Ho Chi Minh City, Vietnam, and taken off to collect only the white part of the husk. Then, the white husk was cut into small species, dried at about 60–70 °C, and ground to powder form. Red mud was collected from Alumin Tan Rai factory (Lam Dong province, Vietnam).

2.2. Preparation of bp-Fe_3O_4

2.2.1. Preparation of Fe_3O_4 hydroxylated particles

Red mud (30 g) was mixed with 700 mL deionized (DI) water in a 1 L beaker and the suspended solution was continuously stirred for 15 min. The supernatant was decanted and repelled water at about 100 °C to collect a red-orange residue of Fe_2O_3 particles. The dry residue was mixed with activated carbon at a mass ratio of 5:1 and conducted an air-limited calcination process at 700 °C for 2 h. The as-obtained product was washed with plenty of DI water and oven-dried at 100 °C to obtain magnetic Fe_3O_4 NPs. Subsequently, the Fe_3O_4 NPs were treated with a 2.5% w/v NH_3 solution (containing 50% ethanol) at 60 °C for 24 h. The final product of Fe_3O_4 hydroxylated (Fe_3O_4–$(OH)_n$) NPs was separated from the solution using an external magnet, followed by washing with DI water and ethanol and dried in ambient air.

2.2.2. Isolation of biopolymers

Biopolymers were extracted from the treated durian husk followed by a previous report (Khan *et al.* 2014) with some modifications. Firstly, an amount of durian husk was mixed with a diluted HCl solution (pH 3) at a ratio of 1/12 (w/v) in a 500 mL two-necked flask. The mixture was then mechanically stirred at 80 °C for 4 h. After the reaction, the solution was hot-filtered to remove the residue. Subsequently, the filtered solution was crystalized by adding a suitable ratio of ethanol, and the residues were washed and stored with ethanol for further use.

2.2.3. Preparation of bp-Fe_3O_4

The as-obtained biopolymers were re-dissolved in 100 mL of DI water (1%, w/v), followed by adding 1 g of hydroxylated-Fe_3O_4 NPs. The mixture was dispersed using ultrasound-assisted and continuous stirring (mechanically) at 90 °C for 30 min. The resultant residue was recovered from the solution followed by a similar route to section 2.2.1. The formed powder was collected as called bp-Fe_3O_4.

2.3. Adsorption test

Batch adsorption experiments were typically carried out in a 50 mL glass bottle containing 20 mL of MB (50 mg/L) and a known amount of each material at pH 7, then the mixtures were continuously shaken at air-ambient temperature for 2 h to reach an equilibrium state. The supernatant solution was then collected from the mixture by using an external magnet and stored at 4 °C for the analysis of MB concentration. Duplicate experiments were done.

The effect of the adsorbent dose was investigated in a range of 1–5 g/L, while other parameters were kept constant. The effect of solution pH on MB adsorption of the nanocomposite was conducted at a pH range of 2 and 8. A suitable diluted HCl or NaOH solution was used for pH adjusting. The kinetic adsorption was conducted with varying adsorption times up to 3 h. The experiments were performed using a series of adsorption solutions at the same experimental parameters with varying predetermined reaction times.

The reusability test of the bp-Fe_3O_4 was performed for seven successive cycles of the MB adsorption–desorption process. The adsorption test was performed as described above. After the adsorption was completed, the MB-laden materials were collected using an external magnet and washed with DI water. The desorption of MB from the material was then performed with 50 mL of 0.1 M EDTA solution for 4 h, followed by subsequent washing with DI water, and ethanol and air-dried, which was ready for the next adsorption test. Note that the magnetic separation was conducted to separate and collect the bp-Fe_3O_4 after each adsorption or desorption process.

2.4. Analysis methods

The prepared materials were characterized using a scanning electron microscopy (SEM; S-4800, Hitachi, Japan), a transmission electron microscopy (TEM; JEM1010, JEOL, Japan), a Fourier transform infrared spectrometer (FTIR; PerkinElmer, Inc., USA), an X-ray diffraction spectrometer (XRD) with monochromatic Cu Kα radiation (D8-Advance; Bruker, Germany), dynamic light scattering (DLS; Horiba SZ-100, Japan), and a vibrating sample magnetometer (VSM; MicroSence EZ9, USA).

The concentration of MB dye in aqueous solutions was determined using a colorimetric method. The absorbance of MB was recorded at a maximum wavelength of 660 nm using a UV/Vis spectrophotometer (Genesys 20, Thermo Scientific, USA).

3. RESULTS AND DISCUSSIONS

3.1. Characterization of the prepared materials

Figure 1 shows an SEM image (a), DLS plot (b), and XRD pattern (c) of the Fe_2O_3 particles recovered from red mud. The SEM image shows an aggregation of Fe_2O_3 with submicron-sized particles, while the DLS plot shows that Fe_2O_3 particles are evenly distributed in a range of between 100 and 250 nm with a mean value of 194.3 nm. The XRD pattern exhibited a series of diffraction peaks at 2θ of 24.1, 33.2, 35.6, 40.9, 54.1, 62.5, and 64.0 can be assigned to the planes of (012), (104), (110), (113), (116), (214), and (300), respectively. These crystalline peaks well agree with the distinctive structure of hexagonal α-Fe_2O_3 crystal of a JCPDS Standard Card No. 89-2810 (Raja *et al.* 2015; Suresh *et al.* 2016; Taghavi Fardood *et al.* 2017; Fouad *et al.* 2019). Figure 2(a) and 2(b) shows the SEM and TEM images of the resultant Fe_3O_4 prepared via carbon combustion of the Fe_2O_3 particles, which were aggregated among the particles and had a particle size of less than 100 nm. In terms of particle size, Fe_2O_3 showed a slightly smaller size compared to Fe_3O_4 based on the SEM images. The combustion process, with its high temperature and anisotropic pressure waves, may have resulted in the aggregation of Fe_3O_4 nanostructures and changes in their morphology (Shin *et al.* 2016). The different sizes between the Fe_2O_3 and Fe_3O_4 particles could be understood by that TEM measures the primary or pristine size of the particles, while the size measured by DLS indicates the secondary or hydrodynamic sizes of particles with surrounding layers in liquid forms. The XRD patterns of the prepared Fe_3O_4 NPs (Figure 2(c)) showed some characteristic peaks assigned at 2θ degrees of 30.3° (220), 35.7° (311), 43.3° (400), 53.5° (422), 57.3° (511), and 62.8° (440). These sharp peaks confirm a good assignment of the crystal structure of Fe_3O_4 NPs, being well consistent with the literature (Loh *et al.* 2008; Silva *et al.* 2013; Zhuang

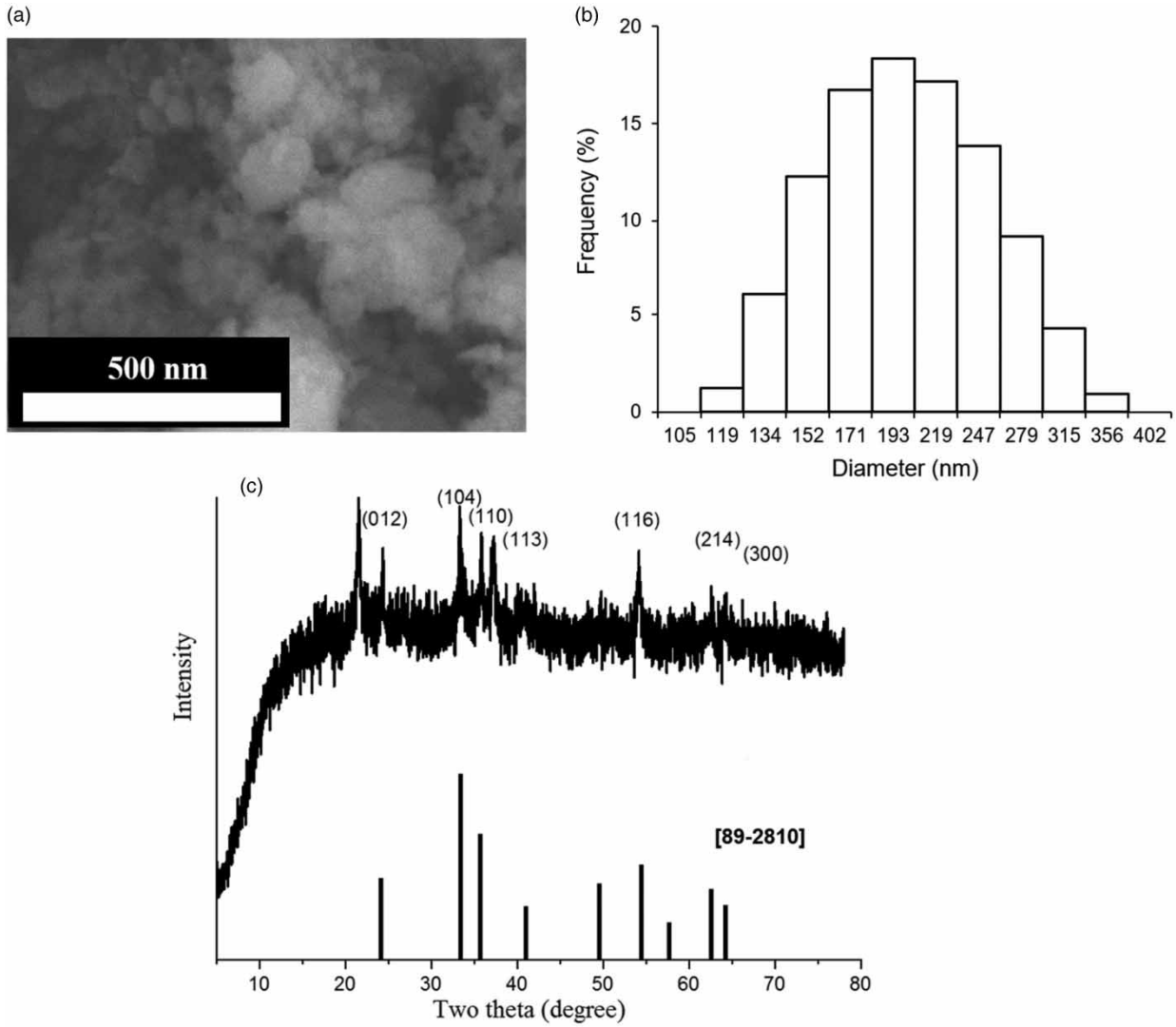

Figure 1 | Characteristics of the Fe_2O_3 nanoparticles: (a) SEM image, (b) DLS size distribution, and (c) XRD pattern (including the XRD pattern of Fe_2O_3 (JCPDS No. 89-2810) for the comparison).

et al. 2015; Bakr *et al.* 2021; Dawn *et al.* 2022). In combustion, carbon as a reducing agent can reduce Fe(III) oxide to lower oxidation states of iron oxides. Parameters such as carbon ratio and oxygen presence could affect the complete reduction of Fe_2O_3 to Fe_3O_4 as reported elsewhere (Molaei *et al.* 2018). In this scenario, Fe_2O_3 NPs underwent the complete reduction to form Fe_3O_4 product and the reaction can be expressed as $3Fe_2O_3\ (s) + C\ (s) \rightarrow 2Fe_3O_4\ (s) + CO\ (g)$. In addition, the color was changed from brown yellow of Fe_2O_3 to dark brown of Fe_3O_4 product after the combustion (data not shown). The FTIR spectrum of the Fe_3O_4 NPs (Figure 3(a)) shows peaks centered at 600.3 and 3,418.3 cm^{-1}, being assigned for Fe–O and O–H stretching vibrations, respectively. Noted, the hydroxylation significantly enhanced the content of O–H functional group of the Fe_3O_4 surface (Figure 3(b)). Overall, the magnetic Fe_3O_4 NPs with chemical reliability were successfully recovered from red mud using a simple calcination process.

Figure 3(d) shows the FTIR spectrum of the bp-Fe_3O_4 compared with those from the biopolymers extracted from the durian husk (Figure 3(c)) and original Fe_3O_4 NPs prepared from red mud (Figure 3(a) and 3(b)). As shown, the bp-Fe_3O_4 appeared to combine the characters of the original biopolymer and Fe_3O_4 NPs. Indeed, the peaks at 2,982.6 cm^{-1} (C–H stretching) and 1,633.6 cm^{-1} (COO– asymmetric stretching) were inherited from the biopolymers, while the assigned peak at 597.81 cm^{-1} was from Fe_3O_4 NPs (Seenuvasan *et al.* 2013; Silva *et al.* 2013; Biswal *et al.* 2016; Ghibaudo *et al.* 2019; Alterary &

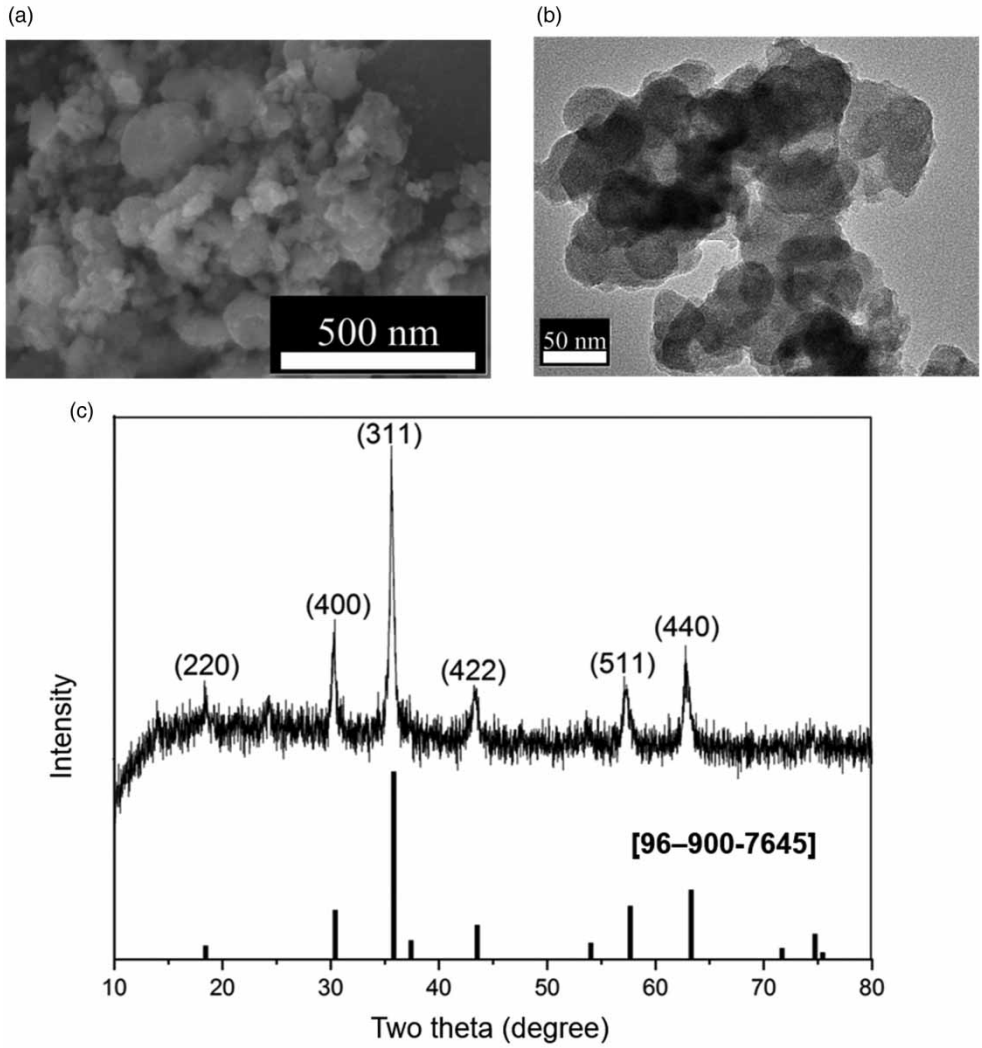

Figure 2 | Characteristics of the Fe_3O_4–$(OH)_n$ nanoparticles: (a) SEM image; (b) TEM image; (c) XRD pattern (including the XRD pattern of magnetite (JCPDS No. 96-900-7645) for the comparison).

AlKhamees 2021; Khashei Siuki *et al.* 2022; Zhang *et al.* 2022). The details of peak characteristics are summarized in Table 1. The results proved the successful incorporation of the Fe_3O_4 and biopolymers to form the bp-Fe_3O_4.

The magnetic properties of the prepared materials were examined by vibrating sample magnetometric analyses. Figure 4 presents the hysteresis loop of the bp-Fe_3O_4 compared with the pristine Fe_3O_4 NPs, observed in a magnetic field ranging from −5,000 to 5,000 Oe at room temperature. As shown, both materials exhibited ferrimagnetic behavior, with almost similar coercivity and remnant magnetization values. Interestingly, the saturation magnetization of bp-Fe_3O_4 (19.84 emu/g) was slightly greater than that of the non-coated ones (18.66 emu/g). Similar phenomena have been reported for magnetic NPs coated with fucan polysaccharides (Silva *et al.* 2013) or with natural rubber latex (Arsalani *et al.* 2018). According to these articles, surface ligands may decrease the interactions among particles, reducing the disorder of surface spins and thus enhancing the magnetization of the formed bp-Fe_3O_4 NPs. Surface properties and particle size are some of the major parameters that can affect the saturation magnetization property of Fe_3O_4 NPs (Nguyen *et al.* 2021). As compared, the saturation magnetization values of the prepared Fe_3O_4 NPs were much larger than magnetized Fe_3O_4 (6.82 emu/g), and Fe_3O_4@Ag (3.52 emu/g) NPs prepared by a thermal method previously reported (Bakr *et al.* 2021). Meanwhile, larger values of saturation magnetization were reported for Fe_3O_4 NPs elsewhere (Silva *et al.* 2013; Zhuang *et al.* 2015; Khashei Siuki *et al.* 2022). Literature reveals that different preparation methods and particle sizes could vary the magnetic properties

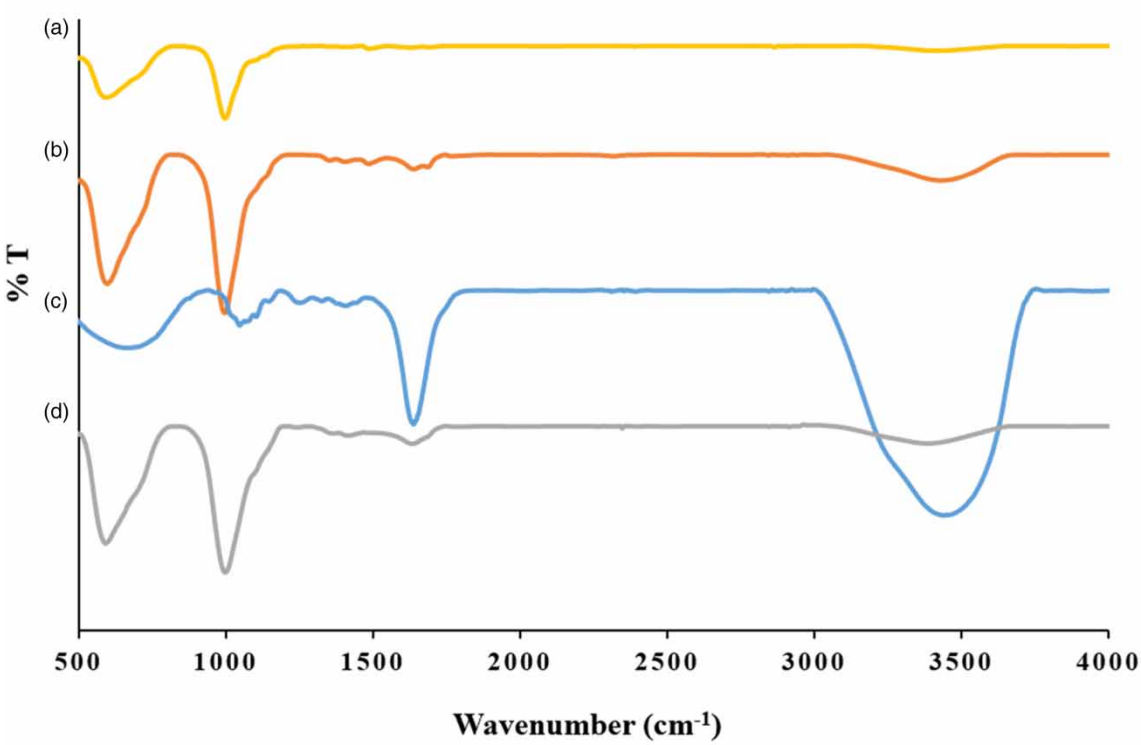

Figure 3 | FTIR spectra of (a) Fe_3O_4, (b) Fe_3O_4–$(OH)_n$, (c) biopolymers, and (d) bp-Fe_3O_4.

of Fe_3O_4 NPs (Bakr *et al.* 2021). It is important to mention that the bp-Fe_3O_4 exhibited rapid and easy recovery from aqueous solutions using an external magnetic field. The outstanding magnetic properties of Fe_3O_4 and bp-Fe_3O_4 NPs rendered them easily manipulated and reusable for water/wastewater treatment.

3.2. Adsorption study

3.2.1. Comparison among adsorbents for the adsorption of MB

Figure 5 shows the removal of MB comparing the bp-Fe_3O_4, Fe_3O_4 NPs, hydroxylated-Fe_3O_4 NPs, and biopolymers adsorbents. These adsorbents exhibited very similar adsorption performance, reaching ~78% of removal at the initial MB concentration and adsorbent dose of 50 mg/L and 1 g/L, respectively. The MB adsorption on the biopolymers was slightly better than bare Fe_3O_4 NPs at the experimental conditions, which consequently resulted in the better adsorption of the bp-Fe_3O_4. The high adsorption efficiency of the biopolymers toward MB dye could be attributed to its major component of pectin (Wai *et al.* 2010; Maran 2015; Kong & Wilson 2020). Indeed, MB species can interact with carboxylic groups (α-galacturonic acid) and/or hydroxyl groups (polysaccharides) of pectin to form pectates through ion exchange or complexation mechanisms (Ilgin 2020). Those well agree with the carboxylate and hydroxyl characteristic peaks examined by the FTIR spectrum (Figure 3(c)). Note that the bp-Fe_3O_4 NPs were selected for further study on the MB adsorption properties because they responded to the good adsorption efficiency, magnetic properties as well as the advantages over each Fe_3O_4 and biopolymer component. Indeed, nano-sized particles (e.g., Fe_3O_4 NPs) often face with engineering problems, such as aggregation effect, difficult manipulation, and risk of leaking of NPs causing a secondary environmental concern (Borm *et al.* 2006); while the biopolymers are less stable and difficult to be separated from the solutions (Ilgin 2020; Kong & Wilson 2020).

3.2.2. Adsorption study of bp-Fe_3O_4

Figure 6 shows the adsorption of MB dye on the bp-Fe_3O_4 examining the effect of (a) solution pH, (b) adsorbent dose, and (c) adsorption time. As shown in Figure 6(a), the MB adsorption on the bp-Fe_3O_4 was dependent on the investigated pH range of 2 and 8. The MB removal was low and stable up to pH 5 (~60%) but significantly increased at pH $\geq$ 6, reaching the maximum adsorption at pH 7 (91.8%). The negligible change of the dye removal in the pH range between 6 and 8 of common real water

Table 1 | FTIR characteristics of the Fe_3O_4, Fe_3O_4–$(OH)_n$, biopolymers, and bp-Fe_3O_4

Spectra	Functional group	Absorption (cm^{-1})
Fe_3O_4	Fe–O	600.3
	O–H	3,420
Fe_3O_4–$(OH)_n$	Fe–O	600.6
	O–H	3,430.8
Biopolymers	COO–	1,406.2
	COO–	1,638.9
	C–H	2,912.2
	O–H for alcoholic and acidic	3,442.0
bp-Fe_3O_4	Fe–O	597.8
	COO–	1,633.6
	C–H	2,982.6
	O–H	3,384.7

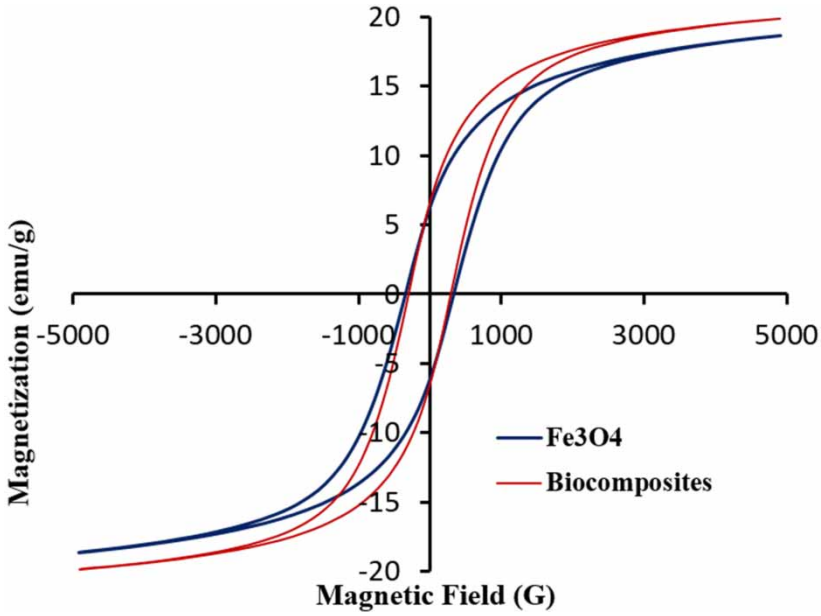

Figure 4 | Vibrating sample magnetometric properties of the pristine Fe_3O_4–$(OH)_n$ and bp-Fe_3O_4 particles.

sources provides an important advantage of practical applications. The solution pH can control the surface charges of adsorbent particles, leading to governing the charge interactions between the cationic MB and active adsorption sites of the adsorbent. In acidic pH (usually $pH < pH_{pzc}$ (point of zero charges, ~6.5 (Milonjić *et al.* 1983))), the functional groups of the bp-Fe_3O_4 (e.g., carboxylic acid and hydroxyl groups) can be predominated in neutral forms or even protonated to form positive surface charges, and thereby were not favorable to adsorb the cationic dye in term of charge interactions. In addition, the presence of an excess H^+ can compete with cationic MB for enrichment on the surface of the bp-Fe_3O_4 (Yu *et al.* 2018). When pH increased beyond pH_{pzc}, the functional groups of the adsorbent became dissociated to increase the extent of negative charges on the adsorbent's surface, which facilitated the electrostatic attraction to the cationic dye (Ilgin 2020). Consequently, the adsorption of MB dye increased. The results were well consistent with literature for the similar biocomposite adsorbents (Alver *et al.* 2020; Bui *et al.* 2021; Ghereghlou *et al.* 2022). Besides, other interactions like hydrogen bonding and dipole–dipole interactions occurring between some functional groups (carboxylic acid and hydroxyl groups) of the adsorbent's surface and dye molecules could be involved in the adsorption mechanisms (Dąbrowski 2001; Parker *et al.* 2012).

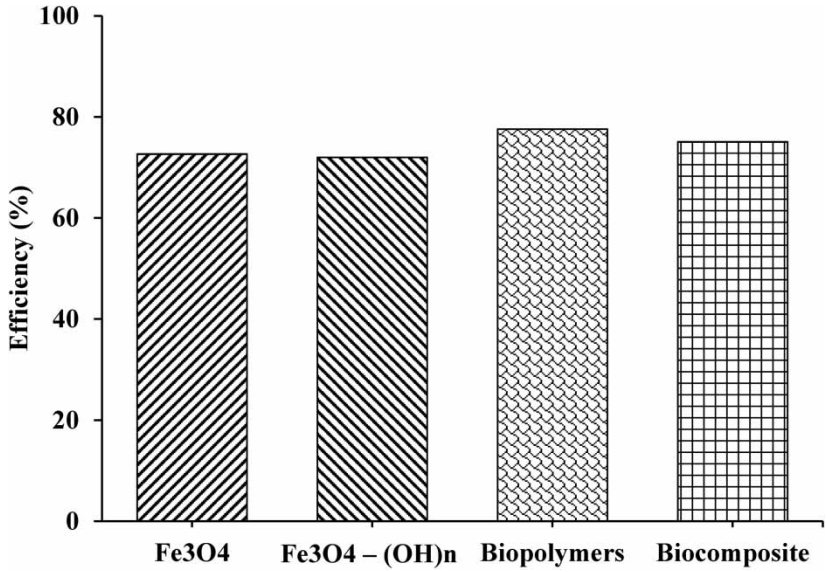

Figure 5 | Methylene blue (MB) adsorption on the bp-Fe_3O_4 compared with the Fe_3O_4, Fe_3O_4–$(OH)_n$, and biopolymers. Experimental conditions: [Adsorbents] = 1.0 g/L, [MB] = 50 mg/L, pH 7, adsorption time of 120 min.

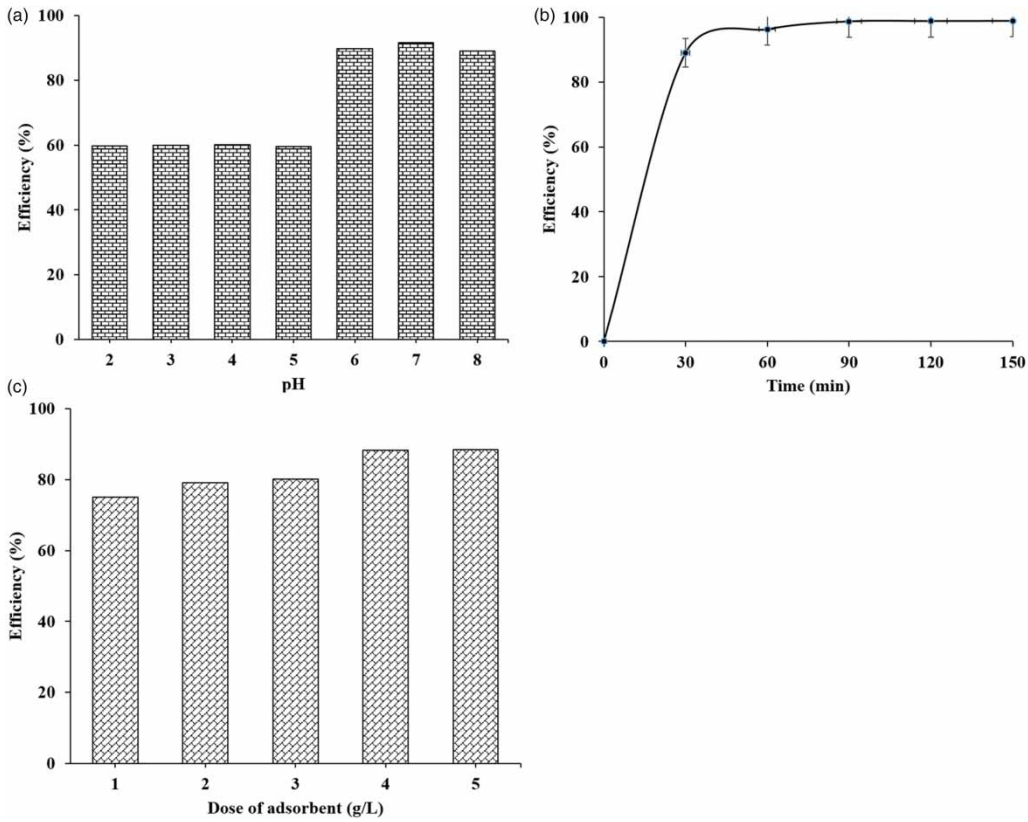

Figure 6 | Effect of (a) solution pH, (b) adsorption time, and (c) adsorbent dose on the MB adsorption of the bp-Fe_3O_4. Experimental conditions: [Adsorbent dose] = 1–5 g/L, [MB] = 50 mg/L, pH 2–8, adsorption time of 0–180 min.

Figure 6(b) shows the MB adsorption on the bp-Fe_3O_4 against time function at pH 7. The removal of MB appeared very fast and reached an equilibrium state within 60 min of the reaction, indicating the fast kinetic adsorption of the bp-Fe_3O_4. When the reaction occurred, the number of active sites on the adsorbent was high enough to ease the adsorption of all MB molecules, resulting in a rapid adsorption rate initially. Further increasing time, the intraparticle diffusion steps into limited adsorption sites made the removal rate for dye molecules become slow and reached an equilibrium state. Overall, the fast kinetic adsorption of MB on the bp-Fe_3O_4 would benefit further process development for practical applications.

The dose of adsorbent is a crucial parameter to evaluate the minimum amount of adsorbent required for effective removal of the dye, and is useful for establishing the experimental conditions to meet the performance goals. Figure 6(c) plots the change of the MB adsorption percentage versus the adsorbent dose ranging between 1 and 5 g/L at the equilibrium condition. The adsorption efficiency increased with increasing the adsorbent load and the adsorbent capacity was in a versus trend (Sharma *et al.* 2011). Indeed, the removal efficiency of MB increased with an increase of the adsorbent dose to 3 g/L. When a dose reached > 4 g/L, the removal efficiency became constant. Generally, an increase in the adsorbent amount resulted in excessive adsorption sites for adsorbing MB dyes and thus, increasing the adsorbed amount of MB dye, while unsaturation of adsorption sites through the adsorption process contributed to the decrease in equilibrium uptake with increasing adsorbent dose (Pooresmaeil *et al.* 2018). Table 2 shows the comparison of equilibrium adsorption capacity between the prepared composite and other similar adsorbents for the adsorption of MB dye.

Table 2 | Comparison of the MB adsorption performance of the bp-Fe_3O_4 to other similar adsorbents in the literature

Adsorbents	q_e (mg/g)	Adsorption parameters ($C_{initial}$ of MB, Adsorbent dose, pH)	Reference
Bp-Fe_3O_4	37.5	50 mg/L, 3 g/L, pH 7	This study
m-ALG/RH	274.9	50 mg/L, pH 6	Alver *et al.* (2020)
Wheat husk	Not mentioned	13.37×10^{-2} mol/L, 25 g/L, pH 6.27	Banerjee *et al.* (2014)
Miswak leaves	60.9	120 mg/L, 1 g/L, pH 10.6	Elmorsi (2011)
Rice husk-activated carbon	9.83	60 mg/L, 12 g/L, pH 6.14	Sharma *et al.* (2011)
Sugar extracted from spent rice biomass	8.3	25–50 mg/L, 2.5–5.0 g/L, pH 5.2	Rehman *et al.* (2012)
Cashew nut shell	5.31	50 mg/L, 20 g/L, pH 10	Senthil Kumar *et al.* (2011)
Neem leaf powder	8.76	25 mg/L, 2 g/L, pH 2–10	Bhattacharyya & Sharma (2005)

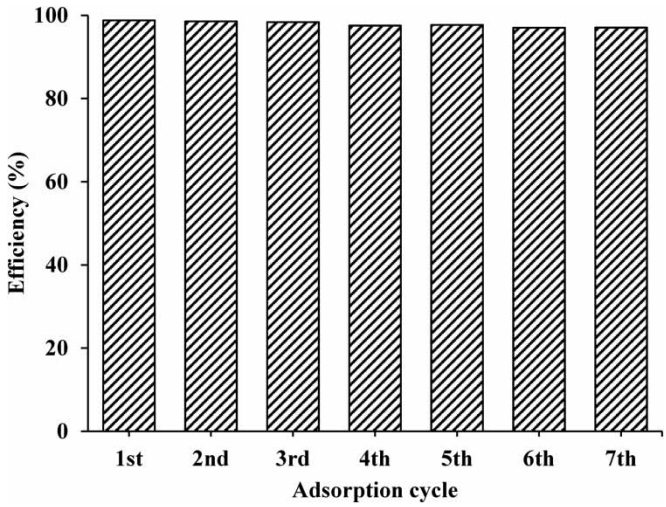

Figure 7 | Reusability test for the adsorption of MB on the bp-Fe_3O_4 during seven adsorption–desorption cycles. Experimental conditions: [Adsorbent] = 4.0 g/L, [MB] = 50 mg/L, pH 7, and 0.1 M EDTA as a desorption solution.

3.2.3. Reusability of the bp-Fe_3O_4

Long-term reusability is an essential parameter to evaluate the feasible economic of an adsorbent for actual applications. Figure 7 presents the adsorption efficiencies of the bp-Fe_3O_4 during seven successive cycles of the MB adsorption–desorption process. Note that the MB desorption was carried out using a solution of EDTA 0.1 M after each step of the adsorption test. The very small decrease in the adsorption efficiency (by only ~1.7%) at the 7th cycle of the adsorption compared with the 1st one suggests the excellent desorption and regeneration of the bp-Fe_3O_4 by the proposed method, indicating long-term reusability. It is important to mention that the magnetic properties of the bp-Fe_3O_4 particles were successfully retained during the tests, allowing them to be separated by applying a magnet.

4. CONCLUSIONS

This study reports the facile preparation of the low-cost magnetic bp-Fe_3O_4 for environmental applications from industrial/agricultural waste sources. The bp-Fe_3O_4 NPs exhibited the combined physicochemical properties of each constituent component and retained the outstanding magnetic properties of the pristine Fe_3O_4 NPs, allowing for easy separation using a suitable magnet. The MB dye adsorption was a fast kinetic reaction and showed effective removal (>90%) at an optimal pH of 7.0 for most natural water sources. Additionally, the material exhibited excellent reusability (by <2% of efficiency decrease) and retained its magnetic property after six regeneration cycles. Further study on the mechanisms of MB adsorption on the bp-Fe_3O_4 as well as its application to real wastewater treatment is necessary.

CREDIT AUTHORSHIP CONTRIBUTION STATEMENT

N.T.B.: Conception and design, experiments and data acquisition and interpretation, Writing – original draft. P.L.N.N.: Data acquisition. Q.-A.T.: Data acquisition. N.T.M.L.: Acquisition of data. T.T.H.: Data acquisition and analysis, Writing – original draft. T.H.B.: Conception and design, data acquisition and interpretation, Writing – review and editing. All authors approved the version of the manuscript to be published.

DATA AVAILABILITY STATEMENT

All relevant data are included in the paper or its Supplementary Information.

CONFLICT OF INTEREST

The authors declare there is no conflict.

REFERENCES

Aksu, Z. 2005 Application of biosorption for the removal of organic pollutants: A review. *Process Biochemistry* **40** (3), 997–1026.

Aksu, Z., Ertuğrul, S. & Dönmez, G. 2010 Methylene blue biosorption by *Rhizopus arrhizus*: Effect of SDS (sodium dodecylsulfate) surfactant on biosorption properties. *Chemical Engineering Journal* **158** (3), 474–481.

Alterary, S. S. & AlKhamees, A. 2021 Synthesis, surface modification, and characterization of Fe_3O_4@SiO_2 core@shell nanostructure. *Green Processing and Synthesis* **10** (1), 384–391.

Alver, E., Metin, A. Ü. & Brouers, F. 2020 Methylene blue adsorption on magnetic alginate/rice husk bio-composite. *International Journal of Biological Macromolecules* **154**, 104–113.

Arsalani, S., Guidelli, E. J., Araujo, J. F. D. F., Bruno, A. C. & Baffa, O. 2018 Green synthesis and surface modification of iron oxide nanoparticles with enhanced magnetization using natural rubber latex. *ACS Sustainable Chemistry & Engineering* **6** (11), 13756–13765.

Ayalew, A. A. & Aragaw, T. A. 2020 Utilization of treated coffee husk as low-cost bio-sorbent for adsorption of methylene blue. *Adsorption Science & Technology* **38** (5–6), 205–222.

Bakr, E. A., El-Nahass, M. N., Hamada, W. M. & Fayed, T. A. 2021 Facile synthesis of superparamagnetic Fe_3O_4@noble metal core–shell nanoparticles by thermal decomposition and hydrothermal methods: Comparative study and catalytic applications. *RSC Advances* **11** (2), 781–797.

Banerjee, S., Chattopadhyaya, M. C., Sharma, U. & Sharma, Y. C. 2014 Adsorption characteristics of modified wheat husk for the removal of a toxic dye, methylene blue, from aqueous solutions. *Journal of Hazardous, Toxic, and Radioactive Waste* **18** (1), 56–63.

Bardajee, G. R. & Hooshyar, Z. 2014 One-pot synthesis of biocompatible superparamagnetic iron oxide nanoparticles/hydrogel based on salep: characterization and drug delivery. *Carbohydrate Polymers* **101**, 741–751.

Bhattacharyya, K. G. & Sharma, A. 2005 Kinetics and thermodynamics of methylene blue adsorption on neem (*Azadirachta indica*) leaf powder. *Dyes and Pigments* **65** (1), 51–59.

Biswal, T., Barik, B. & Sahoo, P. K. 2016 Synthesis and characterization of magnetite-pectin-alginate hybrid bionanocomposite. *Journal of Materials Science & Nanotechnology* **4** (2), 203.

Borm, P. J. A., Robbins, D., Haubold, S., Kuhlbusch, T., Fissan, H., Donaldson, K., Schins, R., Stone, V., Kreyling, W., Lademann, J., Krutmann, J., Warheit, D. & Oberdorster, E. 2006 The potential risks of nanomaterials: A review carried out for ECETOC. *Particle and Fibre Toxicology* **3** (1), 11.

Brunori, C., Cremisini, C., Massanisso, P., Pinto, V. & Torricelli, L. 2005 Reuse of a treated red mud bauxite waste: Studies on environmental compatibility. *Journal of Hazardous Materials* **117** (1), 55–63.

Bui, N. T., Nguyen, V. H., Le, D. T., Tran, T. T. V. & Bui, T. H. 2021 Superparamagnetic cobalt ferric nanoparticles incorporated biopolymers extracted from dragon fruit (*Hylocereus undatus*) peels for nickel(II) removal. *Environmental Technology & Innovation* **23**, 101773.

Dąbrowski, A. 2001 Adsorption – From theory to practice. *Advances in Colloid and Interface Science* **93** (1), 135–224.

Daou, T. J., Pourroy, G., Bégin-Colin, S., Grenèche, J. M., Ulhaq-Bouillet, C., Legaré, P., Bernhardt, P., Leuvrey, C. & Rogez, G. 2006 Hydrothermal synthesis of monodisperse magnetite nanoparticles. *Chemistry of Materials* **18** (18), 4399–4404.

Dawn, R., Zzaman, M., Faizal, F., Kiran, C., Kumari, A., Shahid, R., Panatarani, C., Joni, I. M., Verma, V. K., Sahoo, S. K., Amemiya, K. & Singh, V. R. 2022 Origin of magnetization in silica-coated Fe_3O_4 nanoparticles revealed by soft X-ray magnetic circular dichroism. *Brazilian Journal of Physics* **52** (3), 99.

El-Bindary, A. A., El-Sonbati, A. Z., Al-Sarawy, A. A., Mohamed, K. S. & Farid, M. A. 2015 Removal of hazardous azopyrazole dye from an aqueous solution using rice straw as a waste adsorbent: Kinetic, equilibrium and thermodynamic studies. *Spectrochimica Acta Part A: Molecular and Biomolecular Spectroscopy* **136**, 1842–1849.

Elmorsi, T. M. 2011 Equilibrium isotherms and kinetic studies of removal of methylene blue dye by adsorption onto Miswak leaves as a natural adsorbent. *Journal of Environmental Protection* **2** (6), 817–827.

Fouad, D. E., Zhang, C., El-Didamony, H., Yingnan, L., Mekuria, T. D. & Shah, A. H. 2019 Improved size, morphology and crystallinity of hematite (α-Fe_2O_3) nanoparticles synthesized via the precipitation route using ferric sulfate precursor. *Results in Physics* **12**, 1253–1261.

Ghereghlou, M., Esmaeili, A. A. & Darroudi, M. 2022 Adsorptive removal of methylene blue from aqueous solutions using magnetic Fe_3O_4@C-dots: Removal and kinetic studies. *Separation Science and Technology* **57** (13), 2005–2023.

Ghibaudo, F., Gerbino, E., Copello, G. J., Campo Dall' Orto, V. & Gómez-Zavaglia, A. 2019 Pectin-decorated magnetite nanoparticles as both iron delivery systems and protective matrices for probiotic bacteria. *Colloids and Surfaces B: Biointerfaces* **180**, 193–201.

Hai, L. T. D., Khải, N. M., Quy, T. V. & Huản, N. X. 2014 *Material Composition and Properties of Red Mud Coming From Alumina Processing Plant Tanrai, Lamdong, Vietnam*.

Hokputsa, S., Gerddit, W., Pongsamart, S., Inngjerdingen, K., Heinze, T., Koschella, A., Harding, S. E. & Paulsen, B. S. 2004 Water-soluble polysaccharides with pharmaceutical importance from durian rinds (*Durio zibethinus* Murr.): Isolation, fractionation, characterisation and bioactivity. *Carbohydrate Polymers* **56** (4), 471–481.

Hurairah, S. N., Lajis, N. M. & Halim, A. A. 2020 Methylene blue removal from aqueous solution by adsorption on *Archidendron jiringa* seed shells. *Journal of Geoscience and Environment Protection* **8**, 128–143.

Ilgin, P. 2020 High removal of methylene blue dye from aqueous solution by using a novel pectin-based hydrogel. *International Journal of Environmental Analytical Chemistry* **102**, 1–19.

Kamiya, H., Gotoh, K., Shimada, M., Uchikoshi, T., Otani, Y., Fuji, M., Matsusaka, S., Matsuyama, T., Tatami, J., Higashitani, K., Kurihara, K., Ishida, N., Suzuki, M., Abe, H., Otsubo, Y. & Miyahara, M. 2018 Chapter 3 – Characteristics and behavior of nanoparticles and its dispersion systems. In: *Nanoparticle Technology Handbook (Third Edition)* (Naito, M., Yokoyama, T., Hosokawa, K. & Nogi, K., eds). Elsevier, Amsterdam, pp. 109–168.

Khan, A., Butt, M. S., Randhawa, M., Karim, R., Sultan, M. & Ahmed, W. 2014 Extraction and characterization of pectin from grapefruit (*Duncan cultivar*) and its utilization as gelling agent. *International Food Research Journal* **21**, 2195–2199.

Khashei Siuki, H., Ghamari Kargar, P. & Bagherzade, G. 2022 New Acetamidine Cu(II) Schiff base complex supported on magnetic nanoparticles pectin for the synthesis of triazoles using click chemistry. *Scientific Reports* **12** (1), 3771.

Kong, D. & Wilson, L. D. 2020 Uptake of methylene blue from aqueous solution by pectin–chitosan binary composites. *Journal of Composites Science* **4** (3), 95.

Kuai, S., Zhang, Z. & Nan, Z. 2013 Synthesis of Ce^{3+} doped $ZnFe_2O_4$ self-assembled clusters and adsorption of chromium(VI). *Journal of Hazardous Materials* **250–251**, 229–237.

Liu, X. & Zhang, N. 2011 Utilization of red mud in cement production: A review. *Waste Management & Research* **29** (10), 1053–1063.

Loh, K. S., Lee, Y. H., Musa, A., Salmah, A. A. & Zamri, I. 2008 Use of Fe_3O_4 nanoparticles for enhancement of biosensor response to the herbicide 2,4-dichlorophenoxyacetic acid. *Sensors* **8** (9), 5775–5791. doi:10.3390/s8095775.

Maran, J. P. 2015 Statistical optimization of aqueous extraction of pectin from waste durian rinds. *International Journal of Biological Macromolecules* **73**, 92–98.

Milonjić, S. K., Kopečni, M. M. & Ilić, Z. E. 1983 The point of zero charge and adsorption properties of natural magnetite. *Journal of Radioanalytical Chemistry* **78** (1), 15–24.

Mohebbi, M., Allafchian, A., Jalali, S. A. H. & Kameli, P. 2018 Synthesis and characterisation of Fe_3O_4 at MPTMS at Au nanocomposite by sol–gel method for the removal of methylene blue. *Micro & Nano Letters* **13** (7), 979–984.

Molaei, M. J., Ataie, A., Raygan, S. & Picken, S. J. 2018 The effect of different carbon reducing agents in synthesizing barium ferrite/magnetite nanocomposites. *Materials Chemistry and Physics* **219**, 155–161.

Ngabura, M., Hussain, S. A., Ghani, W. A. W. A. K., Jami, M. S. & Tan, Y. P. 2019 Optimization and activation of renewable durian husk for biosorption of lead (II) from an aqueous medium. *Journal of Chemical Technology & Biotechnology* **94** (5), 1384–1396.

Nguyen, M. D., Tran, H.-V., Xu, S. & Lee, T. R. 2021 Fe_3O_4 nanoparticles: Structures, synthesis, magnetic properties, surface functionalization, and emerging applications. *Applied Sciences* **11** (23), 11301.

Nguyen, T. T. P., Nguyen, V. T., Hoang, N., Hoang, V. D., Luu, X. D., Le, T. M. H., Nguyen, T. H., Hoang, N. B., Tran, T. K. N. & Chu, M. N. 2022 Studies on red mud material to use for combustion of Vietnam pulverized coal. *Inorganics* **10** (5), 58.

Ni, S., Lin, S., Pan, Q., Yang, F., Huang, K. & He, D. 2009 Hydrothermal synthesis and microwave absorption properties of Fe_3O_4 nanocrystals. *Journal of Physics D: Applied Physics* **42** (5), 055004.

Paramguru, R. K., Rath, P. C. & Misra, V. N. 2004 Trends in red mud utilization – A review. *Mineral Processing and Extractive Metallurgy Review* **26** (1), 1–29.

Parker, H. L., Hunt, A. J., Budarin, V. L., Shuttleworth, P. S., Miller, K. L. & Clark, J. H. 2012 The importance of being porous: Polysaccharide-derived mesoporous materials for use in dye adsorption. *RSC Advances* **2** (24), 8992–8997.

Payus, C. M., Refdin, M. A., Zahari, N. Z., Rimba, A. B., Geetha, M., Saroj, C., Gasparatos, A., Fukushi, K. & Alvin Oliver, P. 2021 Durian husk wastes as low-cost adsorbent for physical pollutants removal: Groundwater supply. *Materials Today: Proceedings* **42**, 80–87.

Piga, L., Pochetti, F. & Stoppa, L. 1993 Recovering metals from red mud generated during alumina production. *JOM* **45** (11), 54–59.

Pooresmaeil, M., Mansoori, Y., Mirzaeinejad, M. & Khodayari, A. 2018 Efficient removal of methylene blue by novel magnetic hydrogel nanocomposites of poly(acrylic acid). *Advances in Polymer Technology* **37** (1), 262–274.

Radoor, S., Karayil, J., Jayakumar, A., Parameswaranpillai, J., Lee, J. & Siengchin, S. 2022 Ecofriendly and low-cost bio adsorbent for efficient removal of methylene blue from aqueous solution. *Scientific Reports* **12** (1), 20580.

Rafatullah, M., Sulaiman, O., Hashim, R. & Ahmad, A. 2010 Adsorption of methylene blue on low-cost adsorbents: A review. *Journal of Hazardous Materials* **177** (1–3), 70–80.

Raja, K., Mary Jaculine, M., Jose, M., Verma, S., Prince, A. A. M., Ilangovan, K., Sethusankar, K. & Jerome Das, S. 2015 Sol–gel synthesis and characterization of α-Fe_2O_3 nanoparticles. *Superlattices and Microstructures* **86**, 306–312.

Rehman, M. S. U., Kim, I. & Han, J.-I. 2012 Adsorption of methylene blue dye from aqueous solution by sugar extracted spent rice biomass. *Carbohydrate Polymers* **90** (3), 1314–1322.

Rivas Mercury, J. M., Cabral, A. A., Paiva, A. E. M., Angélica, R. S., Neves, R. F. & Scheller, T. 2011 Thermal behavior and evolution of the mineral phases of Brazilian red mud. *Journal of Thermal Analysis and Calorimetry* **104** (2), 635–643.

Seenuvasan, M., Malar, C. G., Preethi, S., Balaji, N., Iyyappan, J., Kumar, M. A. & Kumar, K. S. 2013 Fabrication, characterization and application of pectin degrading Fe_3O_4–SiO_2 nanobiocatalyst. *Materials Science and Engineering: C* **33** (4), 2273–2279.

Senthil Kumar, P., Abhinaya, R. V., Gayathri Lashmi, K., Arthi, V., Pavithra, R., Sathyaselvabala, V., Dinesh Kirupha, S. & Sivanesan, S. 2011 Adsorption of methylene blue dye from aqueous solution by agricultural waste: Equilibrium, thermodynamics, kinetics, mechanism and process design. *Colloid Journal* **73** (5), 651.

Shahi, M., Sabour, M. R. & Dezvareh, G. A. 2017 Reactive dye extraction utilizing regenerated bleaching earth. *Global Journal of Environmental Science and Management* **3** (3), 299–310.

Sharma, Y. C., Sharma, U. & Upadhyay, S. N. 2011 An economically viable removal of methylene blue by adsorption on activated carbon prepared from rice husk. *The Canadian Journal of Chemical Engineering* **89** (2), 377–383.

Shin, J., Lee, K. Y., Yeo, T. & Choi, W. 2016 Facile one-pot transformation of iron oxides from Fe_2O_3 nanoparticles to nanostructured Fe_3O_4@C core-shell composites via combustion waves. *Scientific Reports* **6** (1), 21792.

Shitu, A. & Ibrahim, A. 2014 Removal of methylene blue using low cost adsorbent: A review. *Research Journal of Chemical Sciences* **4**, 2231–2606.

Silva, V. A. J., Andrade, P. L., Silva, M. P. C., Bustamante D, A., De Los Santos Valladares, L. & Albino Aguiar, J. 2013 Synthesis and characterization of Fe_3O_4 nanoparticles coated with fucan polysaccharides. *Journal of Magnetism and Magnetic Materials* **343**, 138–143.

Sudrajat, H., Susanti, A., Putri, D. K. Y. & Hartuti, S. 2021 Mechanistic insights into the adsorption of methylene blue by particulate durian peel waste in water. *Water Science and Technology* **84** (7), 1774–1792.

Suresh, S., Karthikeyan, S. & Jayamoorthy, K. 2016 Effect of bulk and nano-Fe_2O_3 particles on peanut plant leaves studied by Fourier transform infrared spectral studies. *Journal of Advanced Research* **7** (5), 739–747.

Taghavi Fardood, S., Ramazani, A., Golfar, Z. & Joo, S. 2017 Green synthesis of α-Fe_2O_3 (hematite) nanoparticles using tragacanth gel. *Journal of Applied Chemical Research* **11**, 19–27.

Vangelatos, I., Angelopoulos, G. N. & Boufounos, D. 2009 Utilization of ferroalumina as raw material in the production of ordinary Portland cement. *Journal of Hazardous Materials* **168** (1), 473–478.

Wai, W. W., Alkarkhi, A. F. M. & Easa, A. M. 2010 Effect of extraction conditions on yield and degree of esterification of durian rind pectin: An experimental design. *Food and Bioproducts Processing* **88** (2), 209–214.

Wang, P., Ma, Q., Hu, D. & Wang, L. 2016 Adsorption of methylene blue by a low-cost biosorbent: Citric acid modified peanut shell. *Desalination and Water Treatment* **57** (22), 10261–10269.

Wu, S., Sun, A., Zhai, F., Wang, J., Xu, W., Zhang, Q. & Volinsky, A. A. 2011 Fe_3O_4 magnetic nanoparticles synthesis from tailings by ultrasonic chemical co-precipitation. *Materials Letters* **65** (12), 1882–1884.

Yu, L., Jiang, L., Wang, S., Sun, M., Li, D. & Du, G. 2018 Pectin microgel particles as high adsorption rate material for methylene blue: Performance, equilibrium, kinetic, mechanism and regeneration studies. *International Journal of Biological Macromolecules* **112**, 383–389.

Zhang, N., Liu, X., Sun, H. & Li, L. 2011 Evaluation of blends bauxite-calcination-method red mud with other industrial wastes as a cementitious material: Properties and hydration characteristics. *Journal of Hazardous Materials* **185** (1), 329–335.

Zhang, Q., Cui, W., Guo, H., Wang, B., Wang, H., Zhang, J. & Li, W. 2022 One-pot preparation of nano-scaled magnetic-pectin particles (Fe_3O_4@pectin NPs): Cytotoxicity, antioxidant, and anti-liver cancer properties. *Journal of Experimental Nanoscience* **17** (1), 326–338.

Zhou, L., Huang, J., He, B., Zhang, F. & Li, H. 2014 Peach gum for efficient removal of methylene blue and methyl violet dyes from aqueous solution. *Carbohydrate Polymers* **101**, 574–581.

Zhuang, L., Zhang, W., Zhao, Y., Shen, H., Lin, H. & Liang, J. 2015 Preparation and characterization of Fe_3O_4 particles with novel nanosheets morphology and magnetochromatic property by a modified solvothermal method. *Scientific Reports* **5** (1), 9320.

First received 2 March 2023; accepted in revised form 1 May 2023. Available online 9 May 2023